Implementing digital holograms to create and measure complex-plane optical fields

Angela Dudley
CSIR National Laser center, P.O. Box 395, Pretoria 0001, South Africa and School of Physics, University of the Witwatersrand, Private Bag 3, Johannesburg 2050, South Africa

Nombuso Majola and Naven Chetty
School of Physics, University of KwaZulu-Natal, Private Bag X01, Scottsville, Pietermaritzburg, South Africa

Andrew Forbes
School of Physics, University of the Witwatersrand, Private Bag 3, Johannesburg 2050, South Africa and CSIR National Laser center, P.O. Box 395, Pretoria 0001, South Africa

(Received 4 June 2015; accepted 26 October 2015)

The coherent superposition of a Gaussian beam with an optical vortex can be mathematically described to occupy the complex plane. We provide a simple analogy between the mathematics, in the form of the complex plane, and the visual representation of these two superimposed optical fields. We provide detailed instructions as to how one can experimentally produce, measure, and control these fields with the use of digital holograms encoded on a spatial light modulator.
[http://dx.doi.org/10.1119/1.4935354]

I. INTRODUCTION

Vortex beams are optical fields whose wave-fronts vary along a helical or "twisted" path, resulting in orbital angular momentum (OAM) being carried along the beam's axis.[1] The orbital contribution is defined by the field's azimuthal phase dependence $e^{i\ell\phi}$, where ϕ is the azimuthal angle and ℓ is the azimuthal index, and is equivalent to an angular momentum of $\ell\hbar$ per photon. These vortex-type beams that carry OAM were first experimentally realized as Laguerre-Gaussian (LG) laser modes,[1,2] and a plethora of devices exists for their creation, such as spiral phase plates,[3] "fork" holograms,[4,5] spatial light modulators[6,7] (SLMs), and custom laser resonators.[8] Since their discovery, vortex beams have been applied to strong femtosecond laser pulses[9] and have found applications in optical tweezing,[10] the steering of micro-machines,[11–13] stimulated emission depletion microscopy,[14] non-linear processes in high harmonic generation,[15,16] quantum entanglement,[17–20] and optical communication.[21,22]

Often, when implementing vortex beams in the aforementioned applications, efficient measurement techniques for these OAM-carrying modes are frequently required. It is well known that when a computer-generated hologram, encoded with an ℓ-fold "fork" dislocation, is illuminated with a Gaussian beam, a vortex beam carrying the same "charge" as the hologram (ℓ) is produced in the first diffraction order.[4,5] From the reciprocity of light, an incoming vortex beam of charge ℓ, which is equal to the number of fork dislocations present in the hologram, produces a Gaussian beam in the first diffraction order. By detecting the Gaussian mode (e.g., by using a single-mode fibre that only couples in the Gaussian mode), we can infer the charge of the initial beam from the charge of the hologram.[17] Another solution involves triangular apertures,[23–25] where analysis of the resulting two-dimensional interference pattern denotes the OAM spectrum carried by the beam of interest. Dove prism interferometers[26,27] can be used for the sorting of odd and even OAM modes, and recent work has shown that two diffractive optical elements can be used to transform OAM states into transverse momentum states.[28,29] The latter is capable of measuring any OAM mode as well as superpositions and has successfully been applied to LG and Bessel beams.[30,31] Stokes polarimetery has also shown to be a useful tool in digitally extracting the wavefronts of structured light beams.[32] A more elegant approach capable of determining the intermodal phases between modes in a superposition involves executing an optical inner-product with the field of interest and some match filter encoded as a computer generated hologram, which is known as modal decomposition.[33–35]

Since many classical and quantum optics laboratories require that one has the necessary skills to create and measure superpositions of optical fields (in particular those that carry OAM), we demonstrate how one can implement an SLM to generate and verify such fields. In this paper, we show how to construct a coherent superposition between a Gaussian beam ($\ell = 0$) and an optical vortex that carries a single unit of OAM ($\ell = 1$) with the use of an SLM. In addition, we show how one is able to control the amplitude and phase ratios between the two superimposed modes and how this can be visualized in the complex plane. Once these fields have been experimentally realized, we discuss two separate techniques for extracting the ratio of the constituent components that make up these fields. The first method simply involves using a CCD camera to measure the peak intensities at two adjacent points in the resultant field, while the second method requires an additional SLM to perform a modal decomposition on the resultant field. Although we provide a simple demonstration of the generation and measurement techniques for superimposed optical fields, these methods can be adapted and extended to more complicated scenarios.

The remainder of this paper is organized as follows. In Sec. II, the theory linking the superposition of a Gaussian beam with an optical vortex carrying an OAM value of $\ell = 1$ to the complex plane is developed, and some simple formulas dictating how the amplitude and phase ratios between the two fields can be represented in the complex plane are given. A demonstration of how these fields that occupy the complex plane are generated is provided in Sec. III, which contains

the basic operation of the SLM as well as how the experimental setup is constructed. In Sec. IV, we outline the two measurement techniques and accompany each with a detailed procedure and exemplary results.

II. THEORY: MIXED MODES REPRESENTED IN THE COMPLEX PLANE

In this work, we are interested in the coherent superposition of a Gaussian beam u_{Gauss}, whose 2D and cross-sectional intensity profiles ($I = u^* u$, with * representing complex conjugation) are shown in Figs. 1(a) and 1(d), with an optical vortex u_{vortex}, shown in Figs. 1(b) and 1(e). Mathematically, the superposition of these two fields, depicted visually in Figs. 1(c) and 1(f), can be written as

$$\begin{aligned} u(r,\phi) &= u_{\text{vortex}}(r,\phi) + u_{\text{Gauss}}(r) \\ &= [re^{i\phi} + r_0 e^{i\phi}]G(r), \end{aligned} \tag{1}$$

where $G(r) = e^{-r^2/\omega^2}$ is the standard Gaussian term with beam radius ω, and (r,ϕ) are the spatial (radial and azimuthal) coordinates; r_0, ϕ_0 can be interpreted as the amplitude and phase of the Gaussian mode, respectively.

From basic trigonometry, the polar coordinates (r,ϕ) in Eq. (1) can be re-written in Cartesian (x, y) coordinates: $r = \sqrt{x^2+y^2}$, and $\phi = \arctan(y/x)$, so that our vortex mode can be expressed as $re^{i\phi} = x + iy$. Similarly, writing the Gaussian mode as $r_0 e^{i\phi_0} = x_0 + iy_0$, the superposition field in Eq. (1) can be written

$$\begin{aligned} u(x,y) &= [(x+iy) + (x_0+iy_0)]G(x,y) \\ &= [(x+x_0) + i(y+y_0)]G(x,y). \end{aligned} \tag{2}$$

We see that the amplitude r_0 and phase ϕ_0 of the Gaussian mode manifest itself as an offset $(-x_0, -y_0)$ to the vortex mode. Since the superimposed field in Eq. (2) has real and imaginary parts $(x+x_0)G(x,y)$ and $(y+y_0)G(x,y)$, respectively, we see that the field is displaced along the x-axis by $-x_0$ and along the y-axis by $-y_0$. Where these two contours intersect (at $x = -x_0$ and $y = -y_0$), there is a singularity—a point of zero intensity, and hence undefined phase—about which the phase circulates.

Figure 2 shows an optical field consisting of a Gaussian mode and an $\ell = 1$ vortex mode; the white $\times$ represents the singularity. The location of the singularity can be controlled

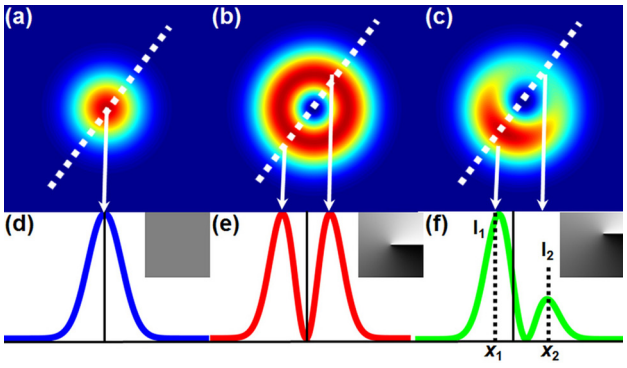

Fig. 1. Top row: 2D intensity profiles of (a) a Gaussian mode, (b) a vortex mode, and (c) a coherent superposition of (a) and (b). Bottom row: the corresponding cross-sectional intensity profiles (plotted across the white dotted lines). Insets denote the corresponding phase profiles.

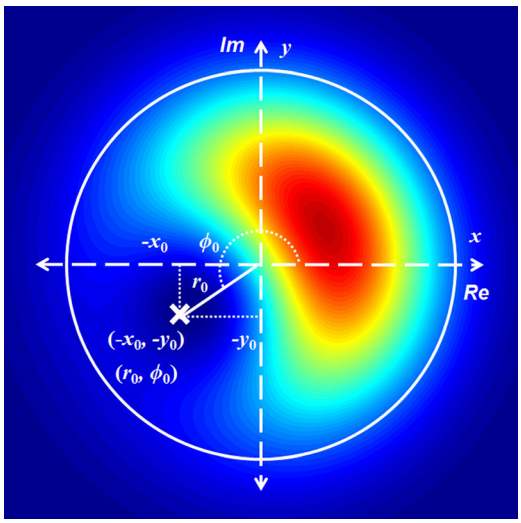

Fig. 2. The complex-plane representation of a superimposed Gaussian ($\ell = 0$) and vortex ($\ell = 1$) mode (i.e., an off-axis vortex). The phase singularity (denoted by the white $\times$) is displaced to the location $(-x_0, -y_0)$ or (r_0, ϕ_0).

by moving the contours $x = -x_0$ and $y = -y_0$ (or equivalently by moving the contours $r = r_0$ and $\phi = \phi_0$) around in the complex plane. Ultimately, by manipulating the amplitude r_0 and phase ϕ_0 between the two superimposed fields, we can control the location of the singularity within the complex plane. Sections III–V will discuss how we can experimentally control the position of the singularity as well as how we can experimentally extract the weightings between the two fields u_{vortex} and u_{Gauss}.

III. CREATING COMPLEX-PLANE FIELDS

Before we delve into the details of experimentally constructing superpositions of Gaussian and vortex modes, a brief overview of the essential optical component, the spatial light modulator (SLM), will be given.

A. Spatial light modulator

Most experimental optics students are aware that the mechanism behind the functioning of SLMs is based on electrically controlled birefringence. We refer those not familiar with this concept to Refs. 36 and 37. Although SLMs offer a plethora of applications, they are not free from efficiency issues. One issue is that the device is unable to diffract the entire incident field into the desired mode. This inefficiency is illustrated in Fig. 3(a), where an azimuthally varying hologram ($e^{i3\phi}$) is illuminated with a Gaussian beam, producing a superposition of the diffracted ($\ell = 3$ vortex) mode and the undiffracted (Gaussian) mode, resulting in the three single-charged vortices moving off-axis. To remove the undiffracted component from the desired, diffracted component, a blazed grating (structured to achieve maximum efficiency in the first diffraction order) is placed over the azimuthal hologram as in the case of Fig. 3(b), producing the well-known "fork" hologram,[4,5] separating the undiffracted zero-order and the diffracted first-order into two independent lateral positions. The function used to encode the fork hologram on the SLM is

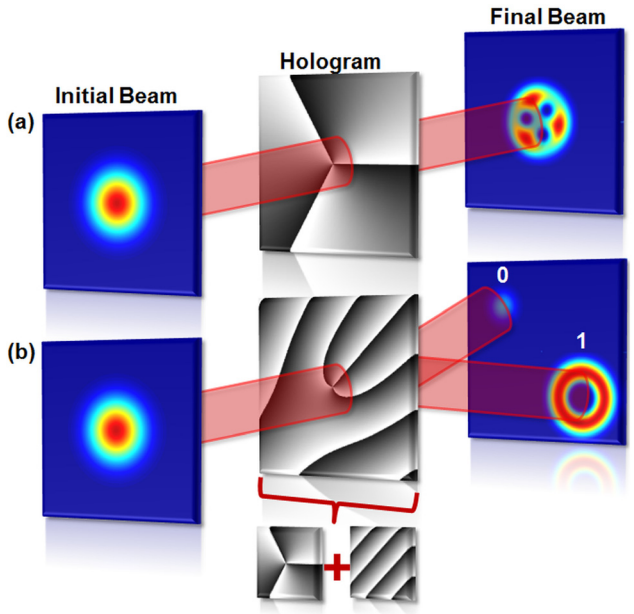

Fig. 3. (a) The azimuthal hologram used to convert a Gaussian beam into a superimposed vortex and Gaussian beam. (b) Overlaying the hologram in (a) with a blazed grating produces a "fork" hologram used to produce the undiffracted Gaussian and diffracted vortex mode in the zero and first diffraction orders, respectively.

$$\ell \arctan\left(\frac{y}{x}\right) + \frac{1}{\Lambda} \mathrm{mod} 2\pi, \tag{3}$$

where Λ defines the grating spacing. The remainder of this work will consider only the fork hologram for generating our fields of interest. Since this article is not dedicated to the functioning of the SLM, readers are directed to past articles in this journal for more detailed and simplified explanations of its capabilities.[38,39]

B. Experimental procedure

Methods to generate superimposed Gaussian and vortex modes include interferometric techniques,[18] where a fork hologram is placed in one of the arms of the interferometer. At the second beamsplitter, the beams in the two arms of the interferometer are superposed. An even simpler technique that we implement here requires displacing the fork hologram with respect to the incident Gaussian beam,[18] the concept of which is illustrated in Fig. 4. Transforming an initial Gaussian mode into a vortex mode ($\ell = 1$) requires that the Gaussian beam be sent through the center of the hologram ($x_0 = 0, y_0 = 0$) where the singularity is located [Fig. 4(a)]. If the beam is shifted to the edge of the hologram, far away from the singularity ($x_0 \to -\infty, y_0 \to -\infty$), the beam is only modified by the blazed grating and the output is again the Gaussian beam [Fig. 4(b)]. By shifting the beam slightly off the center of the singularity in the fork hologram, the singularity in the resulting intensity profile moves off-axis [Fig. 4(c)], similar to the complex-plane representation in Fig. 2. By controlling the horizontal (x_0) and vertical (y_0) displacement of the singularity in the hologram (subsequently r_0 and ϕ_0), the singularity in the intensity profile can be positioned at any point within the complex plane.

The experimental setup for generating these fields is depicted in Fig. 5(a), where a HeNe laser illuminates the

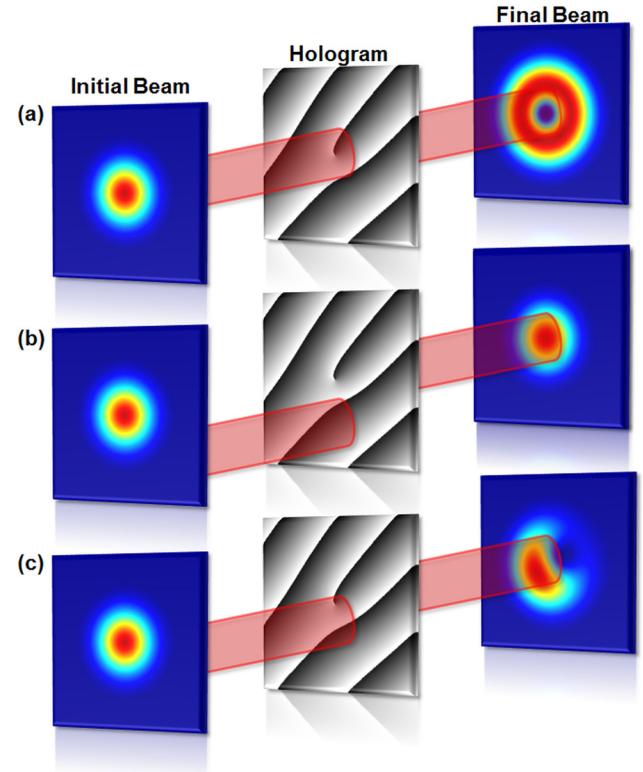

Fig. 4. The concept of how the fork hologram should be illuminated with a Gaussian beam to convert it into (a) a vortex mode, (b) a Gaussian mode, or (c) a mixture of the two.

LCD of a reflective SLM (HoloEye, PLUTO-VIS, with 1920×1080 pixels of pitch $8\,\mu$m and calibrated for a 2π phase shift at $\lambda \sim 633$ nm) encoded with a fork hologram with $\ell = 1$. The first diffraction order at the Fourier plane of the lens L was imaged and magnified onto a CCD camera with the use of the objective O.

C. Experimental results

The displaced-fork hologram in Fig. 6(a), together with the setup shown in Fig. 5(a), was implemented to create complex-plane fields, the results of which are shown in Fig. 6 for movement: (b) along the horizontal axis; (c) along the vertical axis; (d) along a diagonal axis ($y = x$); and (e) around

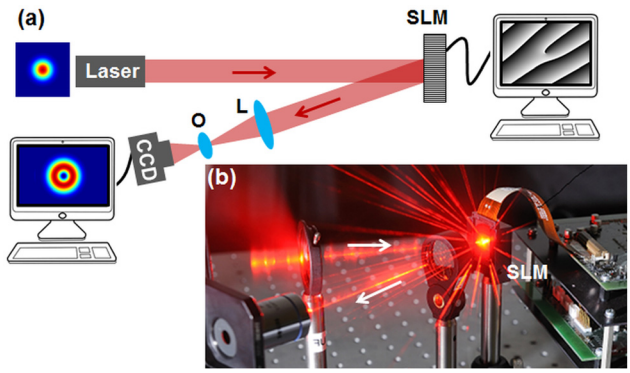

Fig. 5. (a) A schematic of the experimental setup used to create and investigate complex-plane fields (SLM: spatial light modulator; L: lens; O: objective; CCD: CDD camera). (b) Corresponding photograph of the experimental setup.

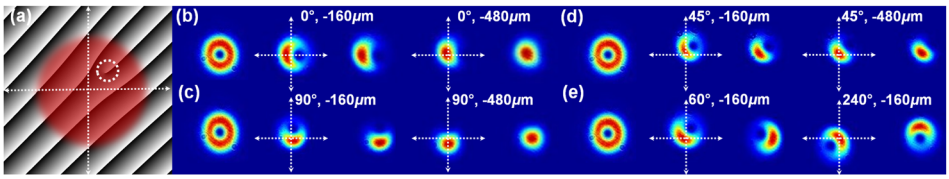

Fig. 6. The intensity profiles of the complex-plane fields where (a) the singularity (marked by the white-dotted circle) in the fork hologram was displaced with respects to the incident beam: (b) along the x-axis, (c) along the y-axis, (d) along the diagonal line $y=x$, and (e) around a circle of radius r. Displacement distances and angles are given as insets for selected examples with respect to a reference point marked by the white dotted cross-hairs (enhanced online) [URL: http://dx.doi.org/10.1119/1.4935354.1].

in a circle. Figure 6, along with the accompanying video, illustrate that it is possible to move the singularity to any position within the complex plane with the aid of the displaced-fork hologram technique.

IV. MEASURING COMPLEX-PLANE FIELDS

Now that one is able to generate fields that map out the complex plane we will study two separate techniques for extracting the fundamental components of these superimposed fields.

A. Method 1: Intensity ratios

1. Concept

It is evident in Fig. 1(f) that as the presence of the Gaussian mode increases, the intensity peak I_1 increases while I_2 decreases. By determining the intensity of the field described in Eq. (2) and solving for $\partial I/\partial x = 0$, the positions x_1 and x_2 associated with I_1 and I_2 in Fig. 1(f) can be determined. Since the particular case of Fig. 1(f) involves a displacement of the singularity along the x-axis only, we can set $y=0$ and $y_0 = 0$. Similarly, if the displacement occurs only along the y-axis, the positions of the intensity peaks y_1 and y_2 can be determined by solving $\partial I/\partial y = 0$, with $x=0$ and $x_0 = 0$. The position for each peak along the x- or y-axis can be expressed as

$$x_{1,2} = \frac{-x_0 \pm \sqrt{x_0^2+2}}{2} \quad \text{and} \quad y_{1,2} = \frac{-y_0 \pm \sqrt{y_0^2+2}}{2}, \tag{4}$$

where, for simplicity, we have taken $\omega = 1$. (The displacements of the singularity in terms of x_0 and y_0 are thus denoted with respect to the beam size ω.)

Substituting the positions for the two intensity peaks into Eq. (2), the intensities I_1 and I_2 can then be determined. By experimentally measuring I_1 and I_2, the ratio of the two modes can be established and compared to the theoretical result

$$\frac{I_2}{I_1} = \left(\frac{x_0 + \sqrt{x_0^2+2}}{x_0 - \sqrt{x_0^2+2}}\right)^2 e^{2x_0\sqrt{x_0^2+2}}, \tag{5}$$

with a similar expression (replacing x_0 by y_0) holding for a displacement in the y-direction. This approach has also been used to analyze small misalignments of an input beam with a very high precision.[40]

2. Experimental results

The ratio I_2/I_1 between the two peak intensities for a range of displacements were measured and are presented in Fig. 7(a) for a displacement of the singularity along the x-axis and in Fig. 7(b) for a displacement along the diagonal line $y=x$. It is evident in Fig. 7 that there is very good agreement between the measured ratios and the theoretical prediction given by Eq. (5). As the singularity in the fork hologram is displaced farther from the center of the incident Gaussian beam, the intensity ratio varies from 0 to 1, denoting the evolution from a pure vortex mode into a pure Gaussian mode with weighted superpositions in between.

B. Method 2: Modal decomposition

1. Executing an optical inner-product

Another method to demonstrate that the off-axis vortex is a superposition of a Gaussian and an $\ell = 1$ vortex mode is to

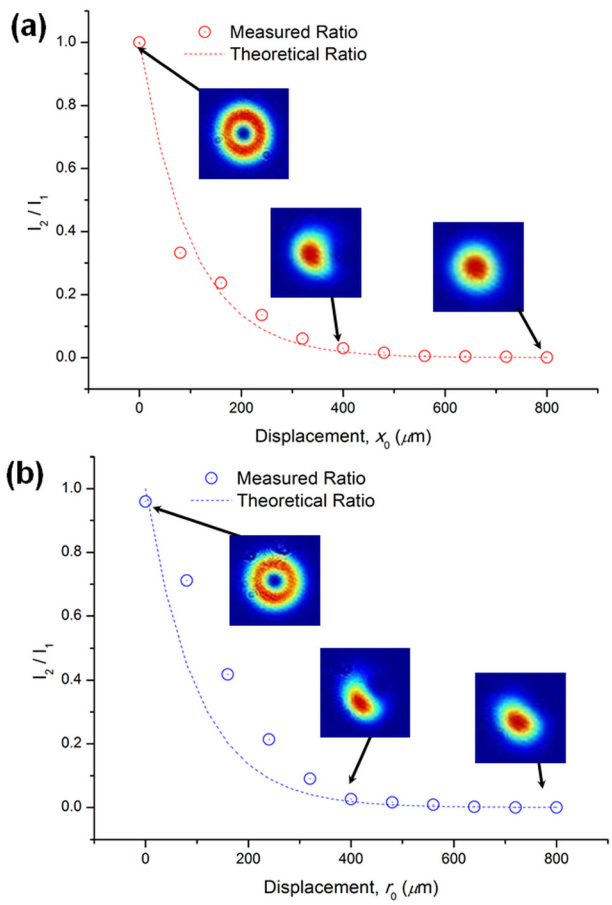

Fig. 7. The ratio of peak intensities plotted against the displacement of the singularity along (a) the x-axis and (b) the line $y=x$. Data points denote measured ratios and dashed curves the theoretically predicted ratio. Corresponding 2D intensity profiles of the modes at selected data points are shown as insets.

project the generated mode onto the orthogonal basis states. Any optical field u can be mathematically expressed in terms of azimuthal modes as $u = \sum c_m e^{im\phi}$. The weightings c_m of the modes can be extracted by performing an azimuthal decomposition by means of an inner-product

$$c_m = \langle u(x,y), t_m(x,y) \rangle = \int\int u(x,y) t_m^*(x,y)\, dx\, dy \tag{6}$$

and is depicted visually in Fig. 8. Here, u denotes the field of interest as given in Eq. (2) and $t_m = e^{im\phi}$ is termed the match-filter. Experimentally, the field u of interest is directed onto an SLM encoded with an appropriate match-filter t_m. The resultant field $U(x,y) = u(x,y)t_m^*(x,y)$ is then Fourier transformed with a thin optical lens from the plane of the SLM to the plane of a CCD detector, as shown in Fig. 8. Here, in the Fourier plane, the Fourier transformation is expressed as

$$\begin{aligned} U_1(k_x,k_y) &= \mathcal{F}[U(x,y)] \\ &= \int\int u(x,y) t_m^*(x,y) e^{-i(k_x x + k_y y)}\, dx\, dy. \end{aligned} \tag{7}$$

The on-axis intensity at the Fourier plane provides an experimental measurement of the optical inner-product in Eq. (6). Setting the propagation vectors to zero ($k_x = k_y = 0$) in Eq. (7), we have

$$\begin{aligned} I_m(0,0) &= |U_1(0,0)|^2 = \left| \int\int u(x,y) t_m^*(x,y)\, dx\, dy \right|^2 \\ &= c_m^2. \end{aligned} \tag{8}$$

When the azimuthal mode index m of the match-filter is the negative of one of the azimuthal modes ℓ present in the field of interest, the weighting c_m of the azimuthal mode will be non-zero, as illustrated in Fig. 8(a). In the case where the azimuthal mode index m is not equal to the negative of one of the azimuthal modes present in the field of interest, the weighting c_m is zero, as illustrated in Fig. 8(b).

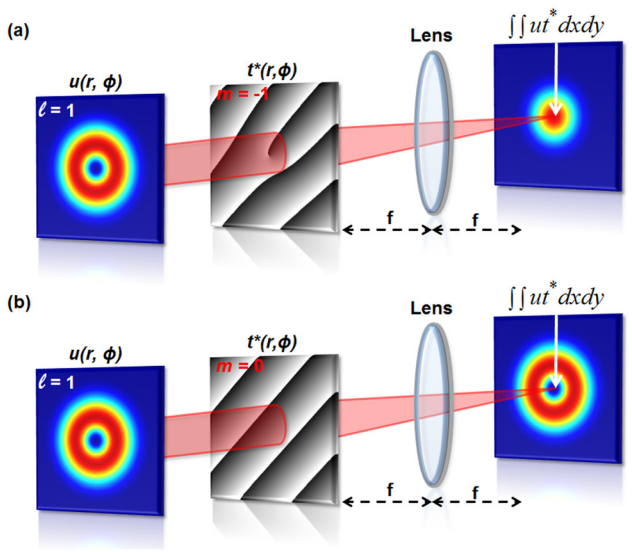

Fig. 8. Schematic of the optical inner-product measurement. (a) Here, the azimuthal mode index ($m = -1$) of the match-filter t_m is the negative of the azimuthal mode ($\ell = 1$) present in the field of interest. The result is a non-zero inner-product, denoted by the bright Gaussian spot. (b) Here, the azimuthal mode index ($m = 0$) is not the negative of the azimuthal mode ($\ell = 1$) present in the field of interest, resulting in a null for the inner-product, denoted by the on-axis singularity.

2. Experimental procedure

The experimental setup to perform an optical inner-product is depicted in the green shaded block in Fig. 9. The field at SLM1 was relay imaged (with the use of lenses L1 and L2) onto SLM2, which was used to find the weightings of the azimuthal modes by performing the inner-product measurement as described in Eq. (6). An aperture in the Fourier plane of SLM1 was used to select the first diffraction order and block all remaining orders. The inner-product was executed experimentally by directing the modes onto the match-filter encoded on SLM2 and viewing the Fourier transform (with the use of lens L3) on the CCD (Spiricon BeamGage, SP620U). The match-filter consists of an azimuthally varying phase $e^{im\phi}$, and by adjusting this phase the various azimuthal weightings in the optical modes can be measured.

3. Experimental results

The weightings of the Gaussian ($\ell = 0$) and vortex mode ($\ell = 1$) for a range of displacements were measured and are presented in Fig. 10 for (a) a displacement of the singularity along the x-axis, and (b) a displacement along the y-axis. It is evident in Fig. 10 that as the singularity in the fork hologram is displaced farther from the center of the incident Gaussian beam, the weighting between the two modes ($\ell = 0$ and $\ell = 1$) varies from 0 to 1, denoting the evolution from a pure vortex mode to a pure Gaussian mode with weighted superpositions in between.

V. APPLICATION: EFFICIENCY CALCULATION

In this section, we will demonstrate with a simple example that the technique of measuring two adjacent intensity peaks as described above can be used as a direct measurement of the diffraction efficiency of an SLM. Let us consider the example given in Fig. 3(a) where an azimuthally varying hologram ($e^{i3\phi}$) possessing no blazed grating is illuminated with a Gaussian beam, producing an on-axis superposition of the unaltered zero order and first order containing the encoded

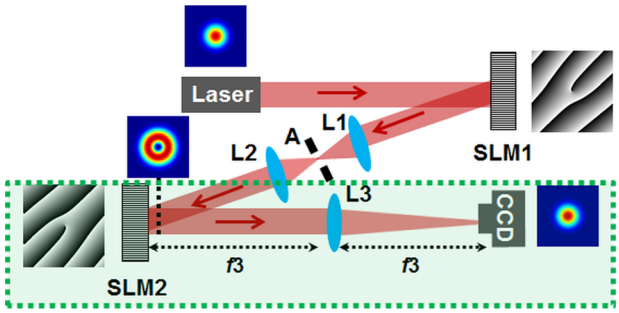

Fig. 9. Schematic of the experimental setup used to create and decompose (denoted by the green shaded block) complex-plane fields (SLM: spatial light modulator; L: lens; A: aperture; CCD: CDD camera). The corresponding holograms for the 2 SLMs (each the complex conjugate of the other, for this particular measurement) and the corresponding 2D intensity profiles at various planes in the setup are shown as insets.

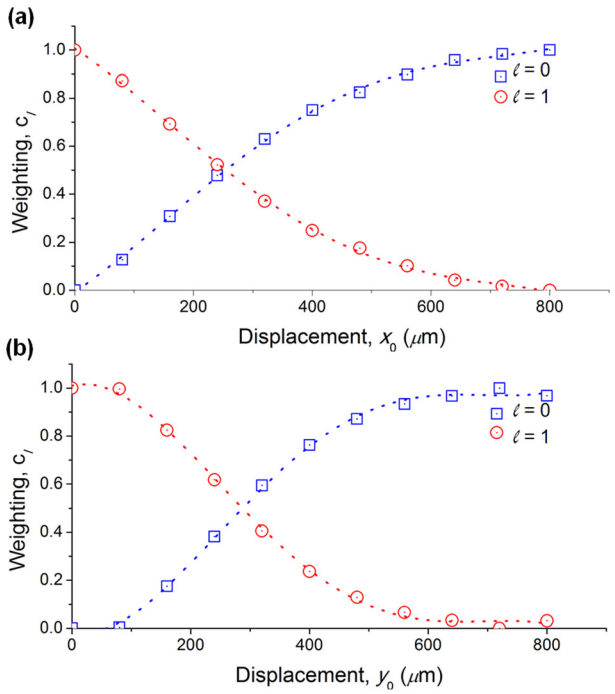

Fig. 10. The weighting of the two azimuthal modes plotted against the displacement of the singularity along (a) the x-axis and (b) the y-axis.

phase profile. The 2D intensity profile of the superimposed mode shown in Fig. 3(a) is depicted in more detail in the complex plane in Fig. 11(a). Here, it is evident that superimposing the vortex ($\ell = 3$) mode with the Gaussian mode results in the phase singularities of unit charge ($\ell = 1$) being displaced to locations such that $x_0 \neq 0$ and $y_0 \neq 0$. To extract the weightings between the two superimposed modes, we first plot its cross-sectional intensity profile [Fig. 11(b)] across one of the peaks and its adjacent null [along the black dotted line in Fig. 11(a)]. By extracting the intensities of the two peaks I_1 and I_2 and making use of Eq. (5), we can directly determine the ratio between the Gaussian and vortex modes. For this particular example, the superimposed mode in Fig. 11(a) consists of 30% Gaussian and 70% vortex. This is illustrated visually in Fig. 11(c) where the two modes have been spatially separated (with the use of a blazed grating) with the Gaussian mode depicted in the zero order (possessing 30% of the energy) and the vortex mode in the first order (possessing the remaining 70%). Although only 70% of the light is projected into the first diffraction order, closer inspection of this mode, shown in Fig. 11(d), illustrates that it is a pure vortex mode, i.e., consisting of 100% vortex mode and 0% Gaussian mode. We can therefore conclude that the SLM used in this example has a diffraction efficiency of 70%. (Please note that we engineered this example to have a poor diffraction efficiency of 70% for illustrative purposes, but in fact most SLMs offer diffraction efficiencies >80%.)

VI. CONCLUSION

In this paper, we have described how one can create an optical field whose position in the complex plane can be controlled with the use of simple digital holograms encoded on a SLM. Most optics labs are equipped with at least one SLM, and so undergraduate and graduate students can get hands-on experience as to how a simple tool can be used to control an optical field's position in the complex plane. Such an experiment will also help students in understanding the fundamental components of an optical field—its amplitude and phase—and how these components manifest in an intensity distribution.

We also show how these fields can subsequently be broken down into their fundamental (Gaussian or vortex) components by either measuring the ratio of the peak intensities at two adjacent points in the field or performing a simple modal decomposition. This form of analysis, particularly in the case of the modal decomposition, provides students with a simple tool to study the constituent components of optical fields. For example, when propagating an optical field through an environment of interest (e.g., a fibre, turbulent atmosphere, etc.), the modal decomposition can be used to decompose the emerging field, thus providing information on the action of the environment (i.e., how it transforms the propagating field). Possessing the tools to create and measure complex optical fields has many applications in research fields including laser beam shaping, quantum optics, and optical tweezing.

ACKNOWLEDGMENTS

N.M. gratefully acknowledges support from the National Research Foundation and the College of Agriculture, Engineering and Science, University of KwaZulu-Natal.

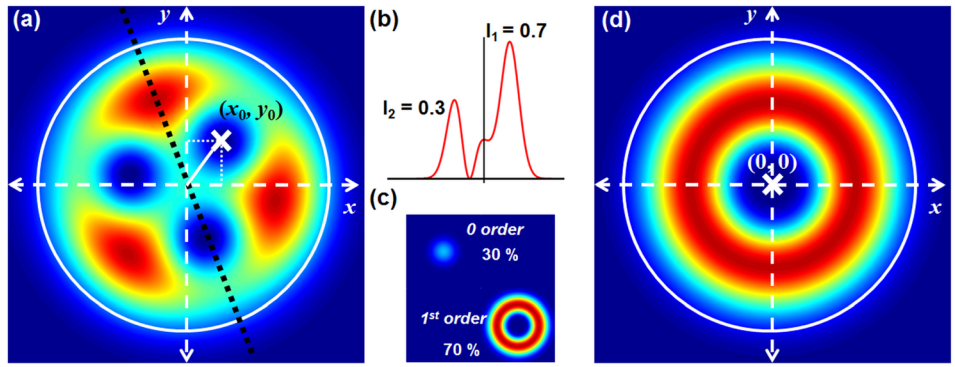

Fig. 11. (a) A 2D intensity profile of a superimposed Gaussian and a vortex mode of $\ell = 3$. Note the displacement of the 3 singularities to off-axis locations in the complex plane. (b) The cross-sectional intensity profile of the mode in (a) plotted along the black dotted line. The intensities I_1 and I_2 give a direct ratio between the two modes (Gaussian: zero diffraction order; vortex: first diffraction order), which provides a direct measurement of the diffraction efficiency. (c) A 2D intensity profile of the separated Gaussian and vortex modes with their corresponding energy in each diffraction order. (d) An enlarged image of the first diffraction order in (c) represented in the complex plane illustrating that the mode is a pure (100%) vortex mode ($\ell = 3$) with a phase singularity located at the origin ($x = 0, y = 0$).

[1]L. Allen, M. W. Beijersbergen, R. J. C. Spreeuw, and J. P. Woerdman, "Orbital angular momentum of light and the transformation of Laguerre-Gaussian laser modes," Phys. Rev. A **45**, 8185–8189 (1992).
[2]M. W. Beijersbergen, L. Allen, H. E. L. O. Van der Veen, and J. P. Woerdman, "Astigmatic laser mode converters and the transfer of orbital angular momentum," Opt. Commun. **96**, 123–132 (1993).
[3]M. W. Beijersbergen, R. P. C. Coerwinkel, M. Kristensen, and J. P. Woerdman, "Helical-wave-front laser-beams produced with a spiral phaseplate," Opt. Commun. **112**, 321–327 (1993).
[4]V. Y. Bazhenov, M. V. Vasnetsov, and M. S. Soskin, "Laser beams with screw dislocations in their wavefronts," JETP Lett. **52**, 429–431 (1990).
[5]N. R. Heckenberg, R. McDuff, C. P. Smith, and A. G. White, "Generation of optical phase singularities by computer-generated holograms," Opt. Lett. **17**, 221–223 (1992).
[6]M. Reicherter, T. Haist, E. U. Wagemann, and H. J. Tiziani, "Optical particle trapping with computer-generated holograms written on a liquid crystal display," Opt. Lett. **24**, 608–610 (1999).
[7]J. E. Curtis, B. A. Koss, and D. G. Grier, "Dynamic holographic optical tweezers," Opt. Commun. **207**, 169–175 (2002).
[8]S. Ngcobo, I. Litvin, L. Burger, and A. Forbes, "A digital laser for on-demand laser modes," Nat. Commun. **4**, 2289-1–2289-6 (2013).
[9]M. Zürch, C. Kern, P. Hansinger, A. Dreischuh, and C. Spielmann, "Strong-field physics with singular light beams," Nat. Phys. **8**, 743–746 (2012).
[10]H. He, M. E. J. Friese, N. R. Heckenberg, and H. Rubinsztein-Dunlop, "Direct observation of transfer of angular momentum to absorptive particles from a laser beam with a phase singularity," Phys. Rev. Lett. **75**, 826–829 (1995).
[11]E. Higurashi, H. Ukita, H. Tanaka, and O. Ohguchi, "Optically induced rotation of anisotropic micro-objects fabricated by surface micromaching," App. Phys. Lett. **64**, 2209–2210 (1994).
[12]P. Galajda and P. Ormosa, "Complex micromachines produced and driven by light," App. Phys. Lett. **78**, 249–251 (2001).
[13]G. Knöner, S. Parkin, V. L. Y. Nieminen, T. A. Love, N. R. Heckenberg, and H. Rubinsztein-Dunlop, "Integrated optomechanical microelements," Opt. Express **15**, 5521–5530 (2007).
[14]K. Willig, S. Rizzoli, V. Westphal, R. Jahn, and S. Hell, "STED microscopy reveals that synaptotagmin remains clustered after synaptic vesicle exocytosis," Nature **440**, 935–939 (2006).
[15]G. Gariepy, J. Leach, K. Kim, T. Hammond, E. Frumker, R. Boyd, and P. Corkum, "Creating high-harmonic beams with controlled orbital angular momentum," Phys. Rev Lett. **113**, 153901 (2014).
[16]C. Hernández-García, A. Picón, J. San Román, and L. Plaja, "Attosecond extreme ultraviolet vortices from high-order harmonic generation," Phys. Rev Lett. **111**, 083602 (2013).
[17]A. Mair, A. Vasiri, G. Weihs, and A. Zeilinger, "Entanglement of the orbital angular momentum states of photons," Nature **412**, 313–316 (2001).
[18]A. Vasiri, G. Weihs, and A. Zeilinger, "Superpositions of the orbital angular momentum for applications in quantum experiments," J. Opt. B: Quantum Semiclassical Opt. **4**, S47–S51 (2002).
[19]B. Jack, J. Leach, H. Ritsch, S. M. Barnett, M. J. Padgett, and S. Franke-Arnold, "Precise quantum tomography of photon pairs with entangled orbital angular momentum," New J. Phys. **11**, 103024 (2009).
[20]M. McLaren, T. Mhlanga, M. J. Padgett, F. S. Roux, and A. Forbes, "Self-healing of quantum entanglement after an obstruction," Nat. Commun. **5**, 3248-1–3248-8 (2013).
[21]G. Gibson, J. Courtial, M. Vasnetsov, M. J. Padgett, V. Pasko, S. M. Barnett, and S. Franke-Arnold, "Free-space information transfer using light beams carrying orbital angular momentum," Opt. Express **12**, 5448–5456 (2004).
[22]J. Wang, J. Yang, I. M. Fazal, N. Ahmed, Y. Yan, H. Huang, Y. Ren, Y. Yue, S. Dolinar, M. Tur, and A. E. Willner, "Terabit free-space data transmission employing orbital angular momentum multiplexing," Nature Photon. **6**, 488–496 (2012).
[23]M. Mazilu, A. Mourka, T. Vettenburg, E. M. Wright, and K. Dholakia, "Simultaneous determination of the constituent azimuthal and radial mode indices for light fields possessing orbital angular momentum," Appl. Phys. Lett. **100**, 231115 (2012).
[24]J. M. Hickmann, E. J. S. Fonseca, W. C. Soares, and S. Chàvez-Cerda, "Unveiling a truncated optical lattice associated with a triangular aperture using light's orbital angular momentum," Phys. Rev. Lett. **105**, 053904 (2010).
[25]A. Mourka, J. Baumgartl, C. Shanor, K. Dholakia, and E. M. Wright, "Visualization of the birth of an optical vortex using diffraction from a triangular aperture," Opt. Express **19**, 5760–5771 (2011).
[26]J. Leach, M. J. Padgett, S. M. Barnett, S. Franke-Arnold, and J. Courtial, "Measuring the orbital angular momentum of a single photon," Phys. Rev. Lett. **88**, 257901 (2002).
[27]M. P. J. Lavery, A. Dudley, A. Forbes, J. Courtial, and M. J. Padgett, "Robust interferometer for the routing of light beams carrying orbital angular momentum," New J. Phys. **13**, 093014 (2011).
[28]G. C. G. Berkhout, M. P. J. Lavery, J. Courtial, M. W. Beijersbergen, and M. J. Padgett, "Efficient sorting of orbital angular momentum states of light," Phys. Rev. Lett. **105**, 153601 (2010).
[29]M. P. J. Lavery, D. J. Robertson, G. C. G. Berkhout, G. D. Love, M. J. Padgett, and J. Courtial, "Refractive elements for the measurement of the orbital angular momentum of a single photon," Opt. Express **20**, 2110–2115 (2012).
[30]A. Dudley, T. Mhlanga, M. Lavery, A. McDonald, F. S. Roux, M. J. Padgett, and A. Forbes, "Efficient sorting of Bessel beams," Opt. Express **21**, 165–171 (2013).
[31]M. P. J. Lavery, D. J. Robertson, A. Sponselli, J. Courtial, N. K. Steinhoff, G. A. Tyler, A. Wilner, and M. J. Padgett, "Efficient measurement of orbital angular momentum over 50 states," New J. Phys. **15**, 013024 (2013).
[32]A. Dudley, G. Milione, R. R. Alfano, and A. Forbes, "All-digital wavefront sensing for structured light beams," Opt. Express **22**, 14031–14040 (2014).
[33]D. Flamm, D. Naidoo, C. Schulze, A. Forbes, and M. Duparré, "Mode analysis with a spatial light modulator as a correlation filter," Opt. Lett. **37**, 2478–2480 (2012).
[34]T. Kaiser, D. Flamm, S. Schröter, and M. Duparré, "Complete modal decomposition for optical fibers using cgh-based correlation filters," Opt. Express **17**, 9347–9356 (2009).
[35]I. A. Litvin, A. Dudley, F. S. Roux, and A. Forbes, "Azimuthal decomposition with digital holograms," Opt. Express **20**, 10996–11004 (2012).
[36]D. Huang, H. Timmers, A. Roberts, N. Shivaram, and A. S. Sandhu, "A low-cost spatial light modulator for use in undergraduate and graduate optics labs," Am. J. Phys. **80**, 211–215 (2012).
[37]J. Davis and I. Moreno, "Generation of laser beams by digital holograms," in *Laser Beam Propagation*, edited by A. Forbes (CRC Press, New York, 2014), p. 175.
[38]A. Carpentier, H. Michinel, and J. Saigueiro, "Making optical vortices with computer-generated holograms," Am. J. Phys. **76**, 916–921 (2008).
[39]B. R. Boruah, "Dynamic manipulation of a laser beam using a liquid crystal spatial light modulator," Am. J. Phys. **77**, 331–336 (2009).
[40]G. Anzolin, F. Tamburini, A. Bianchini, and C. Barbieri, "Method to measure off-axis displacements based on the analysis of the intensity distribution of a vortex beam," Phys. Rev. A **79**, 033845 (2009).